GEOSCIENCE FRONTIERS 2(3) (2011) 449–461

available at www.sciencedirect.com

China University of Geosciences (Beijing)

GEOSCIENCE FRONTIERS

journal homepage: www.elsevier.com/locate/gsf

ORIGINAL ARTICLE

Numerical modelling of structural controls on fluid flow and mineralization

Yanhua Zhang*, J. Robinson, P.M. Schaubs

CSIRO Earth Sciences and Resource Engineering, PO Box 1130, Bentley, WA 6102, Australia

Received 20 January 2011; accepted 16 April 2011
Available online 12 June 2011

KEYWORDS
Structural control;
Dilation;
Fluid flow;
Mineralization;
Numerical modelling;
Shilu Cu-deposit;
Hodgkinson Province

Abstract This paper presents the results of a set of numerical models focussing on structural controls on hydrothermal mineralization. We first give an overview of natural phenomena of structurally-controlled ore formation and the background theory and mechanisms for such controls. We then provide the results of a group of simple 2D numerical models validated through comparison with Cu-vein structure observed near the Shilu Copper deposit (Yangchun, Guangdong Province, China) and finally a case study of 3D numerical modelling applied to the Hodgkinson Province in North Queensland (Australia). Two modelling approaches, discrete deformation modelling and continuum coupled deformation and fluid flow modelling, are involved. The 2D model-derived patterns are remarkably consistent with the Cu-vein structure from the Shilu Copper deposit, and show that both modelling approaches can realistically simulate the mechanical behaviours of shear and dilatant fractures. The continuum coupled deformation and fluid flow model indicates that pattern of the Cu-veins near the Shilu deposit is the result of shear strain localization, development of dilation and fluid focussing into the dilatant fracture segments. The 3D case-study models (with deformation and fluid flow coupling) on the Hodgkinson Province generated a number of potential gold mineralization targets.

* Corresponding author. Tel.: +61 8 6436 8626; fax: +61 8 6436 8555.
E-mail address: Yanhua.Zhang@csiro.au (Y. Zhang).

Peer-review under responsibility of China University of Geosciences (Beijing).
doi:10.1016/j.gsf.2011.05.011

Production and hosting by Elsevier

1. Introduction

It is now recognized that the formation of hydrothermal mineral deposits is often the result of interaction between several key processes including structural (deformation and development of favourable structures), hydrological (fluid flow), thermal (geothermal transport) and geochemical (mineral dissolution and precipitation) processes (e.g. Hobbs et al., 2000; Ord et al., 2002; Zhang et al., 2008). Among these, structural processes represent one type of critical control on mineralization, which have been observed in many regions in the world and are reflected at different scales and in various geological settings.

On a global tectonic scale, there are well-developed theoretical models to explain the association of certain major types of mineral deposits with certain global tectonic settings. For example, there has been a consensus on the formation of world-class orogenic Au-deposits in convergent and accretional orogenic belts at subduction plate margins (e.g. Groves et al., 1998; Goldfarb et al., 2001). It has also been proposed that giant porphyry Cu deposits are often associated with compressively-thickened continental crust with active magmatism (dominantly calc-alkalic), uplift and erosion (e.g. Cooke et al., 2005; Hollings et al., 2005). Such plate tectonic controls represent the first-order controls on the development of globally-significant mineral terrains (provinces), the understanding of which will assist the crucial task of area selection in mineral exploration.

At camp and deposit scales, structural controls are predominantly represented by the development or reactivation of favourable structures due to deformation and the geometrical controls from such structures on the occurrence of mineral deposits or the locations of orebodies. Such structural or geometrical controls have been extensively reported from a large number of regions in the world for a wide range of mineral deposits. Examples of structural controls on mineralization (e.g. fault, thrust-fracture or folds) include: (1) the Silvermines Pb–Zn deposit in Ireland (Taylor, 1984); (2) Mount Carbine W–Sn deposit, Queensland, Australia (De Roo, 1988); (3) Dominique-Peter U deposit, Saskatchewan, Canada (Baudemont and Fedorowich, 1996); (4) Century Zn deposit, Northwest Queensland, Australia (Broadbent et al., 1998); (5) Carlin-type Au deposit in the Gold Bar District, Nevada (Yigit et al., 2003). (6) Au deposits in the Witwatersrand basin (Jolley et al., 2004) and Bendigo, Australia (Schaubs and Wilson, 2002); (7) the Cu–Ag deposits of D. R. Congo (Haest et al., 2007). Studying and understanding of key structural factors controlling mineralization in an area can lead to the determination of exploration targets and the discovery of ore bodies (e.g. Dugdale, 2004; Liu et al., 2010).

The significance of structural controls on hydrothermal ore formation is determined by the theory that structural processes critically affect and control hydrothermal fluid flow (e.g. Oliver, 1996; Hobbs et al., 2000; Zhao et al., 2009). This establishes a theoretical basis for using numerical modelling methods to investigate structural controls on ore formation. Numerical modelling not only has the capability to simulate the interactions of geological structures and rock deformation with fluid flow, but also the flexibility to explore a large number of structural scenarios in a short time frame that can meet the needs of mineral exploration programs. Coupled deformation and fluid flow modelling has been previously used to study favourable structural and fluid flow locations for mineralization in a number of mineral-rich terrains in the world (e.g. Ord et al., 2002; Sorjonen-Ward et al., 2002; Schaubs et al., 2006; Zhang et al., 2007, 2010; Potma et al., 2008; Liu et al., 2010).

This paper focuses on key aspects of structural controls on hydrothermal mineralization and demonstrates the capability of numerical modelling in simulating such controls at outcrop-deposit scales. We first use the results of 2D discrete deformation models and continuum coupled deformation-fluid flow models to illustrate the consistency between the model-predicted patterns and mineralized vein structures observed in nature. We then present the results of a 3D coupled deformation-fluid flow modelling case study on the Hodgkinson Province (North Queensland, Australia), demonstrating how numerical modelling can be used to identify favourable structures for gold mineralization and help gold exploration.

2. Theoretical basis

2.1. Numerical modelling methods

2.1.1. Discrete deformation modelling

Discrete deformation modelling has been carried out using PFC2D (two dimensional Particle Flow Code, also called granular material flow code; Cundall, 2000; Itasca, 2002). In contrast to conventional mesh-based continuum methods, the code simulates a rock domain as a collection of separate circular particles. These rigid particles are bonded together at their contact points in combination with consideration of friction between particles. Under deformation boundary conditions (loading), the full dynamic motion of these particles is simulated, with damping being employed to dissipate kinetic energy.

A PFC granular material assembly consists of many circular particles of various sizes. Each particle is connected through contacts with its neighbouring particles, through which mechanical interactions (forces) between any pair of particles are transmitted. This means that all the mechanical properties of a particle are represented by the lumped mechanical parameters at its contacts with other particles, including normal and shear stiffness, friction and bonding strength. The development of shear zones and fractures are represented by the localization of bond breakage at the contacts.

The motion of particles is governed by Newton's second law. When particles are in contact, contact forces are developed and calculated as a function of displacement between a pair of particles at their contact. The bulk elastic behaviour (stress and equivalent bulk elastic strain) of a particle assembly is determined by normal and shear stiffness of particles. "Plastic" flow of the particle materials is controlled by frictional flow or heterogeneous flow of particles after contact bonds or parallel bonds become broken (Itasca, 2002). The breakage of the bonds is used to determine fracture initiation. For the parallel-bond module, the maximum tensile and shear stresses acting on the bond periphery are calculated. If the maximum tensile stress exceeds the normal bond strength or the maximum shear stress exceeds the shear bond strength, the bond is broken. Multiple domains of particles with varying bond strengths and other contact properties can be used to represent structural complexity.

The Particle Flow Codes, PFC2D and FPC3D, have been calibrated for rocks and other frictional materials by Cundall (2000), Ord et al. (2004) and Suiker and Fleck (2004). The codes have also been applied to the simulation of fracturing and faulting in the upper crust (e.g. Cundall, 2000; Walsh et al., 2001; Zhao et al., 2007).

2.1.2. Continuum coupled deformation and fluid flow modelling

For the continuum deformation and fluid flow models, the two- and three-dimensional finite difference codes, FLAC2D and FLAC3D (Fast Lagrangian Analysis of Continua; Cundall and Board, 1988; Itasca, 2000, 2004) were used. The code is capable of simulating the interactions between deformation and fluid flow in porous media and has been previously used in the simulation of structural processes and controls on fluid flow (e.g. Strayer et al., 2001; Ord et al., 2002; Sorjonen-Ward et al., 2002; Schaubs et al., 2006; Zhang et al., 2006, 2010, 2007; Potma et al., 2008; Liu et al., 2010).

The Mohr–Coulomb isotropic elastic-plastic model (Itasca, 2000, 2004; also see Vermeer and De Borst, 1984; Ord, 1991), one of the constitutive material models in FLAC2D and FLAC3D,

has been adopted for the current models. Under deformation loading, the material with this constitutive behaviour deforms initially in an elastic manner up to a yield point (i.e., before the maximum shear stress reaches a threshold magnitude), after which it deforms plastically; the involved mechanical parameters include shear (G) and bulk (K) elastic moduli, cohesion (C), tensile strength (T), friction angle (ϕ) and dilation angle (ψ). The yield function (f), is defined by:

$$f = \tau^* + \sigma^* \sin\varphi - \cos\varphi, \tag{1}$$

and the plastic potential function (g), is defined by:

$$g = \tau^* + \sigma^* \sin\psi - \cos\psi \tag{2}$$

where $\tau*$ and $\sigma*$ are the maximum shear stress and the mean stress, respectively. The plastic strain-rate ($\dot{\varepsilon}_{ij}$), is given by the flow rule (Malvern, 1969):

$$\dot{\varepsilon}_{ij} = \lambda \frac{\partial g}{\partial \sigma_{ij}} \tag{3}$$

where λ is a constant and σ_{ij} is the stress tensor. Tensile failure occurs when the following condition is met:

$$p - \sigma_{\min} = T \tag{4}$$

where $\sigma_{\min}$ is the minimum principal stress (compressive stress denotes negative, so that tension is positive), p is pore pressure and T is tensile strength.

An important output parameter in the current model is dilation that is expressed as a positive volume change as the result of plastic shearing deformation. The dilatant potential of the Mohr–Coulomb material for plastic deformation is characterized by the dilation angle (ψ). This angle can also be represented in a plot of volumetric strain versus axial strain or shear strain, determined from triaxial tests or shear box tests (e.g. Edmond and Paterson, 1972; Ord, 1991).

Fluid flow in the current models is governed by Darcy's law (Mandl, 1988; Itasca, 2000, 2004), defined for an anisotropic porous medium as:

$$V_i = -k_{ij} \frac{\partial}{\partial x_j}(p + \rho_w g x_i) \tag{5}$$

where V_i is the specific discharge (or flow) velocity, p is the fluid pressure, k_{ij} is the permeability tensor and x_j reflects the positions of a material point, g is gravity and ρ_w is fluid density. Therefore, fluid flow velocities are primarily a function of gradients in fluid pore pressures, and variations in permeability. The hydrological parameters of the models include permeability and porosity. Fluid flow is fully coupled with deformation during the simulation (e.g. Hobbs et al., 2000; Strayer et al., 2001; also see more description in next section).

2.2. Mineralization rate and structural influence

Hydrothermal ore deposit formation is generally related to four key processes including structural (deformation), hydrological (fluid flow), geothermal (thermal transport) and geochemical (chemical reaction, mineral dissolution, transport and precipitation) processes. The formation of an orebody implies that interaction and feedback mechanisms between these processes reinforce one another, resulting in an optimised rate of mineralization. A simplified equation for mineralization rate (Phillips, 1991) can be formulated as below:

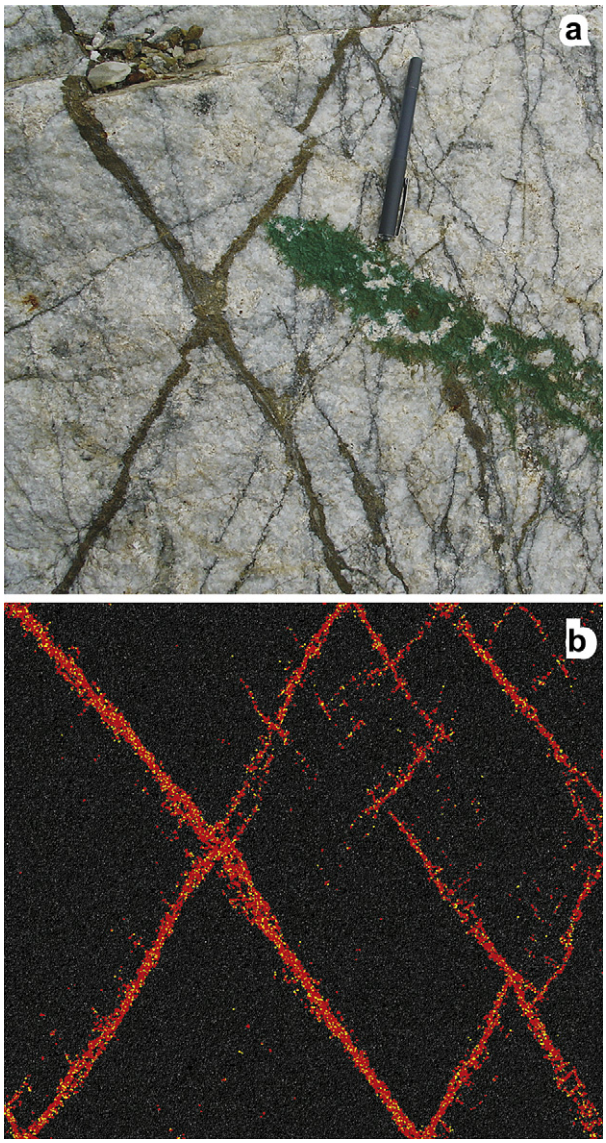

Figure 1 Comparison between (a) the Cu-mineralized vein (fracture) patterns observed at an outcrop on the southeast side of the Shilu Pluton at the Shilu Cu-deposit (Yangchun, Guangdong Province, China; see Fig. 2) and (b) fracture patterns predicted by a PFC2D model. Compressive loading of the model is in the vertical direction. Model-predicted fractures are shown as red and yellow lines, representing the breakage of particle bonds (see more description in the main text). (For interpretation of the references to colour in this figure legend, the reader is referred to the web version of this article.)

$$Q_m = -u \cdot \left\{ \frac{\partial c_e}{\partial T} \nabla T + \frac{\partial c_e}{\partial p} \nabla p + \sum_r \frac{\partial c_e}{\partial c_r} \nabla c_r \right\} \tag{6}$$

where Q_m is the mineralization rate, u is the Darcy fluid velocity, c_e is the equilibrium concentration of a mineral species of interest in the fluid, T is temperature, p is the fluid pressure and c_r are the dissolved concentrations of other chemical species (including hydrogen ions) that influence the reaction of interest. The summation is over the r species that influence the reaction of interest. As such, mineralization rate is a function of fluid velocity

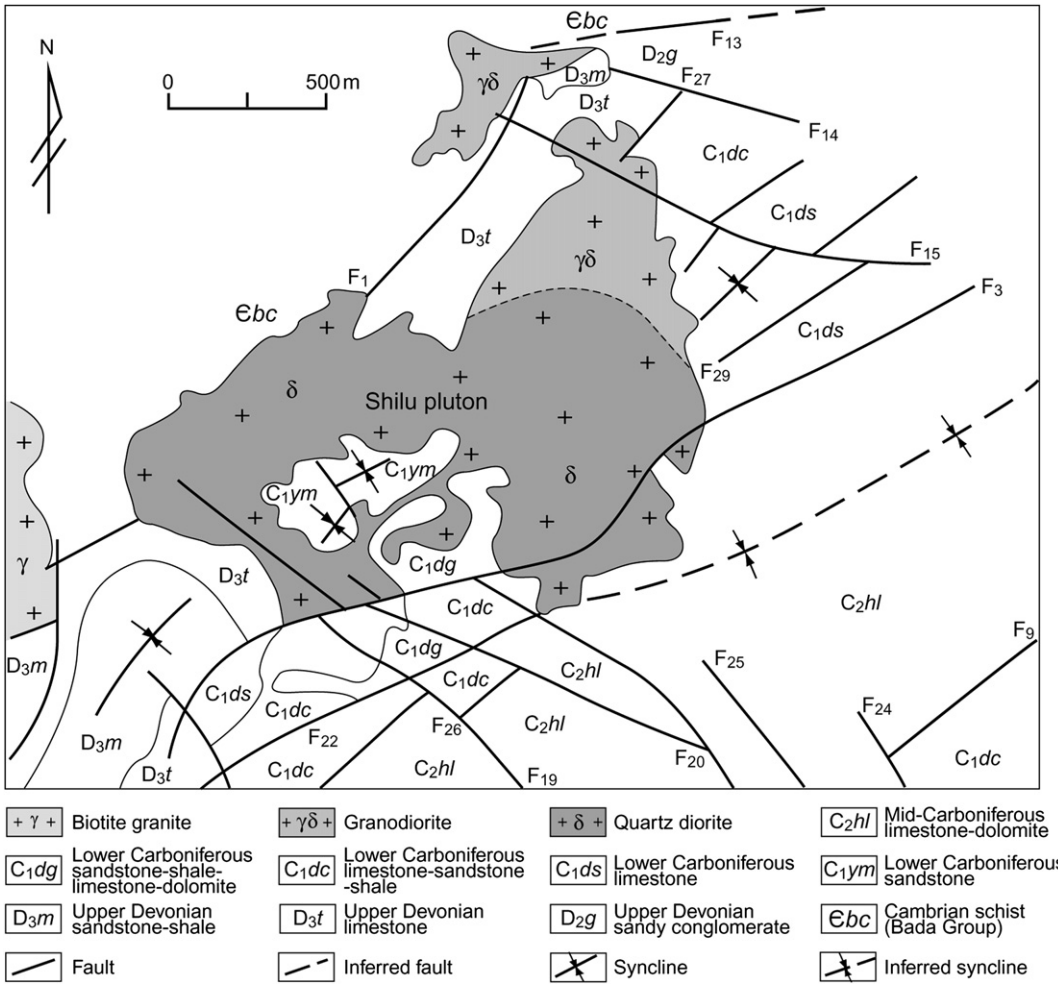

Figure 2 Geological map of the Shilu Cu-deposit in the Yangchun district, Guangdong Province, China (after Luo, 1988). Mineralization at Shilu is predominantly the skarn type governed by the Shilu Pluton (Luo, 1988). Ore bodies are located along and around the contact zones between the Shilu Pluton and Carboniferous-Devonian country rocks (mainly Mid-Carboniferous limestone-dolomite, C_2hl).

and gradients in temperature, fluid pressure and chemical concentrations.

The first-order influences of rock deformation and structural processes on mineralization rate are mainly through their effects on the fluid flow velocity and fluid pressure gradient. These effects can be summarized by three key points. First, rock failure and deformation (strain, ε) will lead to positive volumetric strain or volume increase due to the dilatant nature of rock deformation as described by Mohr–Coulomb mechanical behaviour (e.g. Edmond and Paterson, 1972). This will lead to a drop in fluid pore pressure (often shown as fluid focussing) and the generation of large variations in pore pressure and fluid flow velocity gradients at these sites with strain localization and dilation according to the equation:

$$\Delta p = K_w \varepsilon_v \tag{7}$$

where Δp is fluid pore pressure changes, K_w is fluid bulk modulus and ε_v is volumetric strain. Second, rock deformation may enhance the permeability (k in equation (5)) of rocks and structures (e.g. faults) and hence fluid flow velocities. Third, deformation may generate large changes in structural framework such as topographic elevation or depression, and hence leads to major variations in the pore pressure or head distribution of an area.

Figure 3 A photo showing the geometrical features of a set of Cu-mineralized veins on the southeast side of the Shilu Pluton at the Shilu Cu-deposit (Yangchun, Guangdong Province, China; see Fig. 2). Note large thickness variations along irregularly-curved veins.

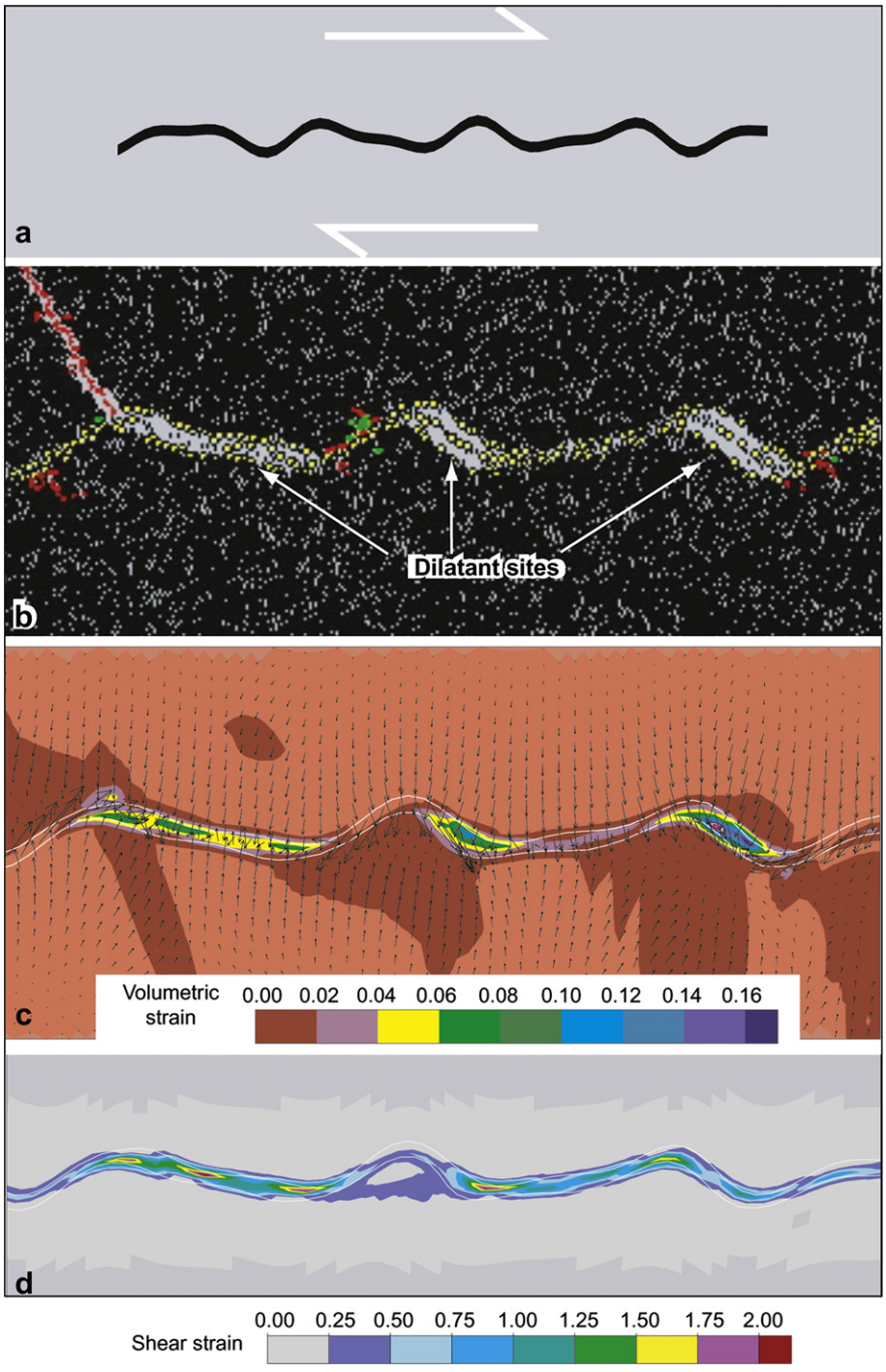

Figure 4 The results of 2D numerical models simulating shearing deformation along a pre-existing curved fracture. (a) Initial geometries of 2D numerical models (only the central portion of the model is shown). Arrows illustrate the direction of shearing in the models. (b) Fracture patterns and void (dilation) distribution derived from a discrete PFC2D model. (c) Volumetric strain patterns (dilation as positive volumetric strain values) and instantaneous fluid flow velocities surrounding a pre-existing fracture, predicted by the 2D coupled deformation and fluid flow model (the maximum fluid flow velocity is 2×10^{-6} m/s). (d) Shear strain distributions along the pre-existing fracture in the deformation and fluid flow model.

3. Prediction of structurally-favourable locations for mineralization: simple models

3.1. A discrete deformation model

Mineralized veins represent one type of mineralization structure widely observed in many ore deposits. Fig. 1a shows a set of Cu-mineralized veins observed at an outcrop in the Shilu Cu-deposit (Yangchun, Guangdong Province, China; Fig. 2). The Cu-veins occur along a set of conjugate fractures, illustrating clear evidence of structural control on ore deposition. The question addressed in this work is whether such basic outcrop-scale mineralization structures can be simulated and predicted by numerical models. We have chosen the 2D discrete numerical modelling method (PFC2D) for this numerical modelling test due to the potential involvement of discrete fractures.

The 2D PFC model is a square-shaped particle assembly with an initial size of 20 cm by 20 cm (Fig. 1b), similar to the size of the observed area of the Cu-veins at the Shilu Cu-deposit (Fig. 1a). Since the model aims to simulate the virtual situation of a natural example, radius sizes of the particles in the numerical sample have been defined to be in the range of 0.2–0.3 mm, consistent with grain sizes of the Gosford sandstone (Edmond and Paterson, 1972; Ord, 1991). The numerical sample contains 177,234 particles, with a density of 2226 kg/m^3, consistent with that of the sandstone. The other micro mechanical parameters include parallel-bond normal stiffness and shear stiffness (both 1.16×10^{10} Pa/m), parallel-bond normal and shear bonding strengths (both 3.5×10^6 Pa), and a friction coefficient of 1.0. The numerical sample is deformed under biaxial compression conditions. A loading rate (compression) in the vertical direction is gradually applied to the top and bottom of the sample, while the vertical sides of the sample are confined by a constant confining pressure of 10 MPa.

In the PFC model, the development of shear bands and fractures is reflected by the patterns of bond breakage between particles. Fig. 1b illustrates the patterns of shear bands and fractures (red colour locations) in the numerical granular material sample after 5% bulk shortening. It is noted that multiple, conjugate shear zones and fractures are well developed at this stage, with deformation and fracture clusters predominantly localised along conjugate shear zones. There is a remarkable similarity between the Shilu Cu-vein pattern (Fig. 1a) and the shear band and fracture pattern predicted by the PFC model (Fig. 1b). This similarity is not only reflected by the orientation relationship of conjugate veins and shear bands, but also by the consistency in their widths. Some detailed geometrical features along and around the two major conjugate veins and shear bands also match remarkably well (see the top-central area of Fig. 1a and b).

Two goals have been achieved by the PFC model. First, it demonstrates that the discrete granular-material flow modelling with relatively simple bonding mechanical rules can realistically simulate the development of the outcrop-scale mineralized vein structure as illustrated in Fig. 1a. Second, the model also confirms the importance of structural controls on such vein-type mineralization, i.e., the initiation and development of fractures in response to mechanical loading can lead to the localized deposition of ore minerals.

3.2. Comparison of a discrete deformation model and continuum coupled deformation-fluid flow model

In this section, we demonstrate the consistency between the results of a discrete deformation model and a continuum coupled deformation and fluid flow model in the explanation and prediction of occurrence of structural-controlled mineralization. Fig. 3 illustrates the pattern of another Cu-vein structure observed at another outcrop in the Shilu Cu-deposit (see Fig. 2). The morphologies of the veins exhibit curved geometries for "primitive" fractures and considerable variations in the thickness of Cu-mineralized veins. The question is, "what is the key structural factor governing the formation of such vein features?"

A discrete deformation model using PFC2D and a correlating continuum deformation-fluid flow model using FLAC2D, both two dimensional, have been constructed to explore this question. Both models simulate a rectangular area of 20 m (horizontal) by 14 m (vertical), containing a pre-existing curved fracture (see Fig. 4a for a portion of model geometry). The PFC2D model consists of 70,000 particles (particle radius sizes in the range of 1.6–2.35 cm), with a density of 2250 kg m^{-3}, stiffness (normal and shear) of 1.4×10^9 Pa/m, bonding strength (normal and shear) of 2.5×10^6 Pa, and a frictional coefficient of 0.05. The pre-existing fracture in the PFC2D model is assigned with a zero bonding strength. As such, the fracture's strength is only controlled by friction and therefore represents a weakness which easily slips. The FLAC2D model has the same density but involves a different set of mechanical and hydrological parameters for the computation of coupled deformation and fluid flow (see Table 1). The parameters for the fracture also define a zone of weakness. Both models are deformed under a dextral (top-to-right) shearing and plain-strain condition as illustrated in Fig. 4a.

Fig. 4b shows fracturing and damage patterns around the pre-existing fracture in the PFC2D model at a bulk shear strain of 0.05. It is noted that even a small bulk shear has led to noticeable dextral (top-to-right) shearing along the pre-existing fracture. The shearing movement generated large dilation (void formation) along certain segments of the fracture. These dilatant segments all dip towards the shearing direction of the rock block above the fracture and hence represent pull-apart sites along the fracture. These segments remain dilatant throughout shearing. It is also noted that tensile cracks develop near the apex (or "hinge") of the fracture curvatures, about 45° to the shearing direction, reflecting the effect of dextral-shearing generated tension.

The FLAC2D model is also deformed to a similar bulk shear strain to the PFC2D model. The patterns of volumetric strain, shear strain and fluid flow velocities are presented in Fig. 4c and d. Positive volumetric strain (volume increase) gives a quantitative prediction of structural dilation. Major dilation sites clearly occur

Table 1 Material properties of the FLAC2D model.

Model unit	Density (kg m^{-3})	Bulk modulus (Pa)	Shear modulus (Pa)	Cohesion (Pa)	Tensile strength (Pa)	Permeability (m^2)	Porosity	Friction angle (°)	Dilation angle (°)
Host rock	2250	2.33×10^{10}	1.4×10^{10}	1.5×10^7	7.5×10^6	2.0×10^{-16}	0.2	30	2
Fracture	2100	4.762×10^9	4.35×10^9	1.0×10^6	0.5×10^6	2.0×10^{-15}	0.2	10	2

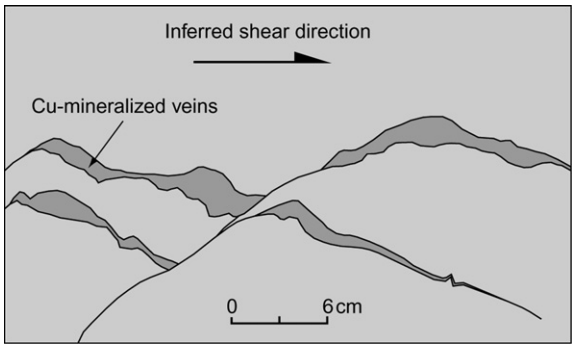

Figure 5 Inferred kinematic direction (top-to-right shearing) for the Cu-mineralized vein structures shown in Fig. 3. It is suggested that the thicker segments of the Cu-veins represent pull-apart segments along curved fractures under top-to-right shearing.

along those segments of the fracture which represent the pull-apart portions resulting from dextral shearing. These are consistent with the locations of major void formation in the PFC2D model (Fig. 4b). In contrast, low volumetric strain is localized along the compressional slopes of fracture curvatures. It is also noted that dilational segments coincide approximately with the distribution of higher shear strain (Fig. 4d). The distribution of instantaneous fluid flow velocities (Fig. 4c) indicates that there is strong focussing of fluid into the dilatant segments of the fracture. This reflects a strong interaction between deformation and fluid flow during coupled structural-hydrological processes. While recognizing the effect of the hydrological process on the mechanical response of deforming rocks (e.g. facilitating mechanical failure due to the effects of pore fluid pressure), such interaction is likely dominated by structural or mechanical processes. This indicates that shear strain and mechanical damage generate dilation at structurally-favourable sites, which immediately generates the response of the fluid pore pressure field (pore pressure drop according to equation (5)) and leads to fluid focussing and also possibly mixing towards dilation sites. The enhancement of permeability with rock deformation and dilation is another important factor affecting fluid flow, which has not been considered in this model.

The modelling results above provide some insight into how the Cu-vein structure shown in Fig. 3 was formed. We can speculate that the rocks at this outcrop were most likely subjected to local dextral (top-to-right) shearing along a pre-ore deposition fracture (Fig. 5). Such a local kinematic framework could lead to the pull-apart and dilation of certain segments of fractures and hence generates favourable structural sites for ore fluids to localize and mix. These segments could host Cu-mineralized veins, with the thickness of veins likely reflecting the magnitude of dilation.

The current results show that both the discrete deformation (PFC2D) model and continuum coupled deformation-fluid flow (FLAC2D) model can explain the key structural controls on the formation of Cu-veins illustrated in Fig. 3. However, the coupled deformation and fluid flow model can provide more insights into fluid flow fields, while still capturing the major features of discrete fracture and void formation from the discrete deformation model in the form of quantitative shear strain and dilation distributions. Such continuum models make direct use of macro-properties from laboratory tests, allowing the reconstruction of reasonably-complex geological structures, and simulating spontaneous interactions between structural and fluid flow processes. It therefore represents an appropriate modelling tool for application to practical mineral exploration.

4. A case study: application of coupled deformation-fluid flow modelling to mineral exploration

The remaining objective of this paper is to demonstrate the applicability of coupled deformation and fluid flow modelling to mineral exploration. We present a 3D coupled deformation-fluid flow modelling case study on the Hodgkinson Province, North Queensland, Australia. The numerical results have been used to identify key favourable structures for gold mineralization and exploration targets for the region.

4.1. Description of regional geology and exploration task

The Hodgkinson Province is a strongly deformed turbidite-filled basin located in the far north of Queensland or north-east corner of the Australian continent (Fig. 6). The stratigraphy of the basin sequences consists of Silurian-Devonian sandstone, siltstone and shale with minor volcanics, conglomerate, chert and limestone. A study of the structural history (e.g. Zucchetto et al., 1999; Davis et al., 2002) identified several major deformation events: D_1 (Middle Ordovician, E–W shortening, slaty cleavage development), D_2 (Late Ordovician, E–W shortening), D_3 (Early Permian, NE–SW to E–W extension), and D_4 (Permian, E–W to ENE–WSW shortening, representing the main contractional phase of the Hunter-Bowen Orogeny with major granitoid emplacement). Three dominant structural trends are observed in the Hodgkinson Province (Fig. 6), as the preserved signatures of the deformation events above. The N–S trending structures are represented by foliations, D_2 fault zones (Davis et al., 2002), and also the Palmerville Fault (Vos and Bierlein, 2006) that bounds the region in the west. Two other major structural trends include NW-trending faults (also called the Desailly structure, see Davis et al., 2002), and NNW-trending shear zones and faults.

Gold mineralization in the Hodgkinson Province likely occurred prior- or syn-D_4. Davis et al. (2002) suggested the timing of D_4 mineralization at 280–240 Ma (Permian), but Vos and Bierlein (2006) proposed two gold-forming episodes for the southeast part of the Province (i.e., Northcote area) during ~370–300 Ma. The province has a long history of gold production from several small to medium sized gold deposits (e.g. Tregoora, Kingsborogh, Northcote deposits; see Fig. 6), and exploration has recently been renewed. Previous studies (Davis et al., 2002; Vos and Bierlein, 2006) suggested that gold mineralization in the region is structurally controlled, mostly localized along a network of NNW to NW-trending faults.

To assist exploration efforts in the region, the current numerical modelling study has been carried out as an application of numerical simulation techniques. The study is divided into two phases: the first reverse engineering phase aims at developing an improved understanding of the structural conditions that led to the localisation of gold-bearing fluids within known deposits across the province, and the second predictive phase aims to use this understanding to predict new targets of potential mineralization as well as ranking targets within known gold-bearing systems.

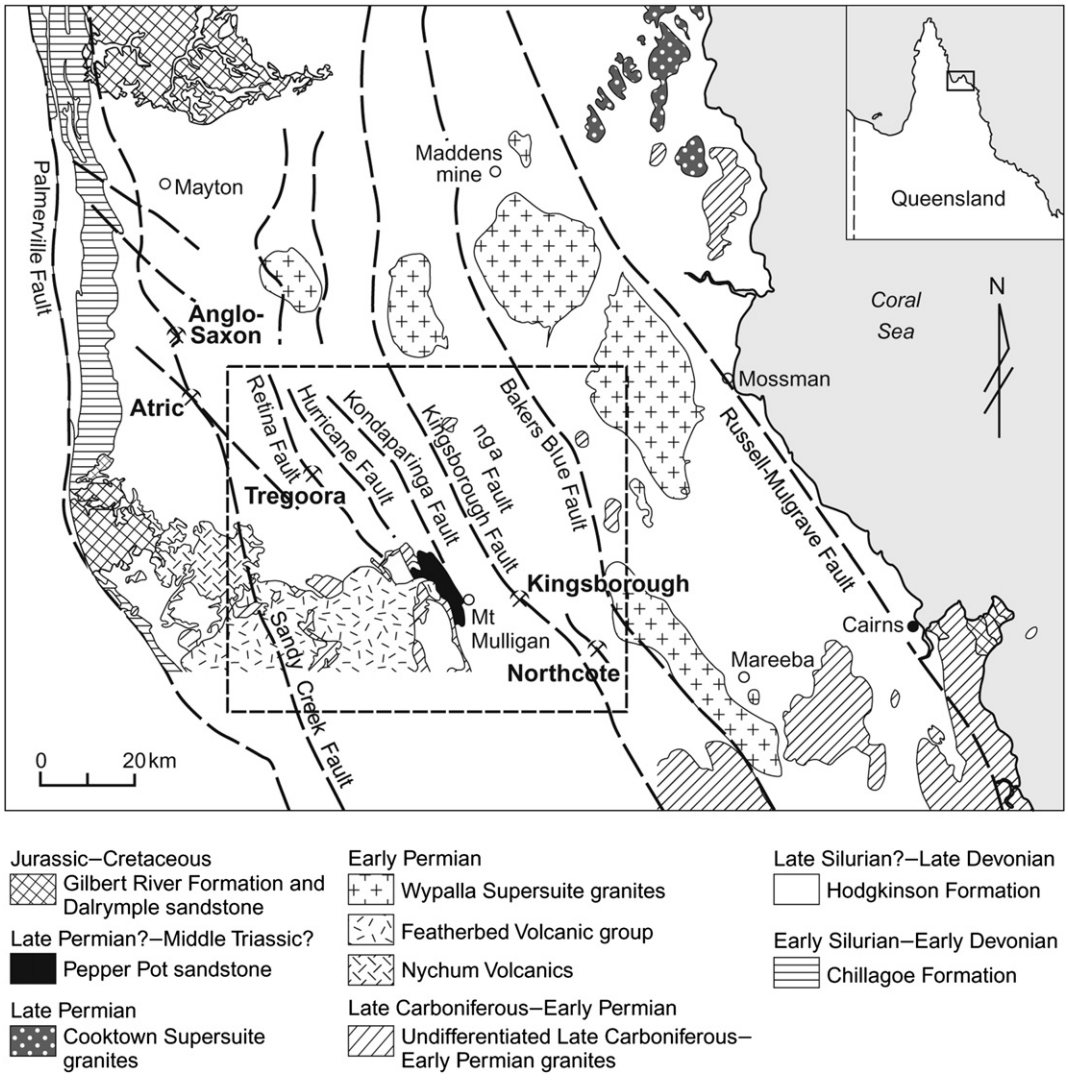

Figure 6 A simplified geological map for the Hodgkinson Province, showing location of the region (inset), orientations of major faults (based on the 3D geological model of Geological Survey of Queensland, Australia) and geological boundaries (simplified from Davis et al., 2002). The dash-line box outlines the area of the Hodgkinson Gold Field reverse engineering model. Anglo-Saxon, Atric, Tregoora, Kingsborough and Northcote are the main gold deposits in the region.

4.2. Numerical modelling approach with a mineral exploration focus

The 3D geological model of the Hodgkinson Province constructed by the Geological Survey of Queensland (Fig. 7) provides the main basis for the current numerical modelling study. The other data required for the model was collected from published literature, Geological Survey of Queensland maps and data, Republic Gold Ltd data and fieldwork in the Hodgkinson gold field. These studies focussed on identifying the conditions during mineralization within known systems and developing a conceptual understanding of the controls on mineralization. The critical constraints are the present architecture of the system and at the time of mineralization; depths at which the mineralization occurred; behaviour of rocks within the system; timing of mineralization, relative to granitic magmatism and metamorphism; and kinematic constraints.

In the reverse engineering phase, the modelling effort is aimed at identifying the most likely model (e.g. regional deformation orientation) conditions which can lead to the prediction of the known deposits in the region, by performing a series of model simulations on the known gold deposits (termed reverse-engineering modelling). Such models include those on the Hodgkinson gold field (with the Tregoora, Kingsborough and Northcote deposits). In the regional predictive phase, information learnt from the first phase was applied to the whole regional-scale model to predict prospective targets in the region.

4.3. Modelling results and development of exploration targets

4.3.1. Reverse-engineering modelling on the Hodgkinson gold field

The Hodgkinson gold field is an area located in the central part of the Hodgkinson Province (see the dash-line box in Fig. 6), which contains a number of known gold deposits (Tregoora, Kingsborough and Northcote) and mineralized sites. Analyses of the existing data suggest that most of the gold mineralization in the

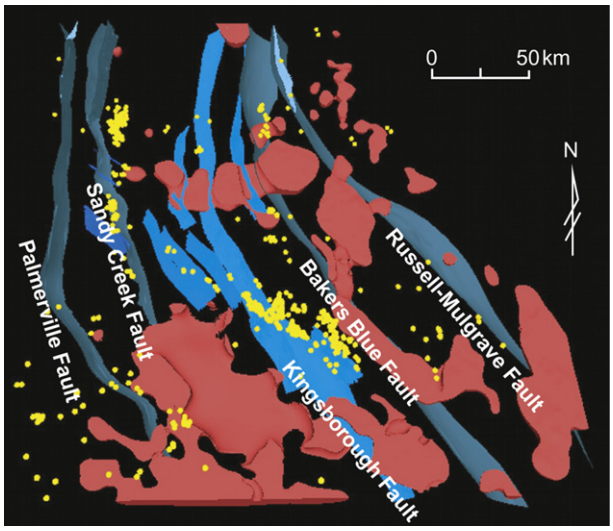

Figure 7 Top-down view of the 3D geological model developed by the Geological Survey of Queensland, Australia. Included in the model are major faults (light blue lines), granites (red), and gold deposits and mineralization (yellow). (For interpretation of the references to colour in this figure legend, the reader is referred to the web version of this article.)

Hodgkinson Province occurred prior to or during sinistral strike-slip or an oblique-slip movement (D_4 or earlier) on many of the steeply-dipping, NW- to NNW-trending faults. However, the detailed nature of such sinistral transcurrent, or sinistral transpressional kinematic orientations is difficult to determine. Therefore, the aim of the reverse-engineering modelling was to test a wide range of possible kinematic orientations and to determine the most likely orientation associated with gold mineralization in the field. The rationale is that gold mineralization at Tregoora, Kingsborough and Northcote is clearly structurally or fault-reactivation controlled, and hence the kinematic orientation that can result in optimal localizations of strain and fluid flux at these locations in a model should reflect the most likely kinematic orientation associated with mineralization.

The 3D numerical models consider a fault array consisting of NW- to NNW-trending faults (see fault traces in Fig. 8; also see Figs. 6 and 7) within a homogeneous host rock package. The model properties are given in Table 2 (i.e., for faults and average host rock). A series of kinematic orientations (such as sinistral transpression with various directions for the normal contractional component) were tested as model deformation boundary conditions. Such kinematic orientations (model boundary conditions) are achieved by the application of various combinations of E–W and N–S deformation velocity components to the model vertical edges, which represent the resolved velocity components of an assumed regional deformation transport vector (regional stress orientation). The model top is simulated as a "free" surface buried to a 5 km depth level (i.e., confining stresses on the surface reflect a 5 km overburden); the model base is fixed in the vertical direction (free in the horizontal direction but cannot move up and down). Model interior areas are free to move in any directions according to local deformation conditions.

The results (Fig. 8) show that the optimal model results are from that simulating a regional stress field characterized by sinistral transpression with an ENE-70° (2:1 strike slip to compression ratio) direction of the normal contractional component. For this model, the optimal localizations of shear strain and fluid flux occur on three NW- to NNW-trending faults, and all three locations coincide with the locations of the Tregoora, Kingsborough and Northcote gold deposits. Therefore, it is inferred that the syn-mineralization regional stress field for the Hodgkinson Province is most likely a sinistral transpressional regime with the normal contractional component oriented at ENE-70°.

4.3.2. Regional predictive modelling on the Hodgkinson Province

The regional-scale 3D deformation and fluid flow model (Fig. 9) for the Hodgkinson Province was constructed, based on the structural data from the Hodgkinson 3D geological model of the Geological Survey of Queensland (Fig. 7). The model, 310 km (E–W) by 250 km (N–S) by 8.4 km (thickness) in size, simulates a series of faults with various strike-lengths and irregularly-curved fault geometries and a simplified stratigraphic sequence consisting of 4 rock units (see Table 2 for model properties). The model top is assumed to be located at a depth of 5 km. The host rock is treated as a simplified rock unit for basin rocks (mainly metasediments) where mechanical properties are averaged. This "average" sedimentary unit is the main host to faults, together with granite and crystalline basement rocks (west of the Palmerville Fault).

The granite in the models is simplified from the geometries of the 3D geological model (Fig. 7), with the modelling parameters on those assumed to be pre-mineralization. These granites are

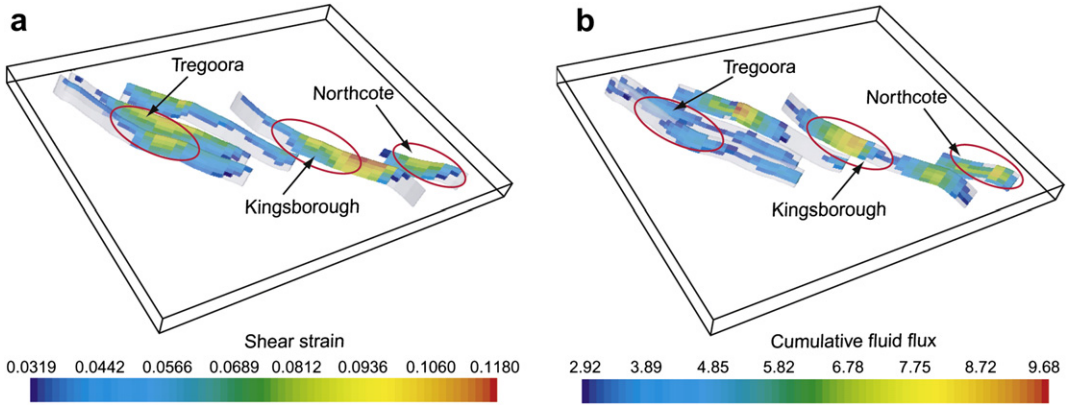

Figure 8 Results of the Hodgkinson gold field reverse-engineering models. (a) and (b) plots of shear strain and cumulative fluid flux distribution patterns, respectively. Locations of the Tregoora, Kingsborough and Northcote gold deposits are approximately marked by red circles. (For interpretation of the references to colour in this figure legend, the reader is referred to the web version of this article.)

Table 2 Material properties of the 3D model for the Hodgkinson Province.

Model unit	Density (kg m^{-3})	Bulk modulus (Pa)	Shear modulus (Pa)	Cohesion (Pa)	Tensile strength (Pa)	Permeability (m^2)	Porosity	Friction angle (°)	Dilation angle (°)
Faults	2500	2.3×10^{10}	1.3×10^{10}	2.5×10^{7}	2.0×10^{6}	1.0×10^{-16}	0.01	20	3
Average host rocks	2500	1.985×10^{10}	6.5×10^{9}	2.97×10^{7}	3.805×10^{6}	1.0×10^{-17}	0.01	30	2
Granite	2700	3.6×10^{10}	1.7×10^{10}	6.0×10^{7}	6.0×10^{6}	1.0×10^{-18}	0.01	40	5
Basement	2800	4.66×10^{10}	2.8×10^{10}	5.0×10^{7}	5.0×10^{6}	1.0×10^{-19}	0.01	30	5
Chillagoe Formation	2500	3.33×10^{10}	2.0×10^{10}	5.06×10^{7}	5.0×10^{6}	1.0×10^{-18}	0.001	30	3

interpreted to have intruded pre- to syn-deformation and mineralization (Vos and Bierlein, 2006). As such, the granites may be important in localising strain, fluid flow and hence mineralization. In the models, the top boundaries of these granites are situated at approximately 1 km below the model top. The Chillagoe Formation is a rock unit in the 3D geological model, consisting of basaltic, carbonate and/or dolomitic rocks, and exposed between the Sandy Creek and Palmerville Faults (Fig. 9). The stratigraphic package described above represents a system with more permeable faults in less permeable host rocks.

The 3D coupled deformation and fluid flow modelling was performed using the regional stress field determined from the reverse engineering modelling, i.e., sinistral transpression with compressional component at ENE-70° and with a 2:1 strike-slip to compression ratio. Shear strain distributions and cumulative (total) fluid flux patterns were visualized for the ~2% shortening stage, and are projected onto the regional geological map (Fig. 10). It is noted that the locations of known gold deposits or mineralized sites are all reflected by shear strain anomalies and cumulative fluid flux anomalies. This can be viewed as a validation for the regional scale model on the basis of the distribution of mineralization. Moreover, a series of other areas are also highlighted by anomalously high distribution of shear strain and fluid flux. A number of potential gold mineralization targets can be identified according to these anomalies (Fig. 10). Similar to the sites of known deposits and mineralization, the locations of these targets are all distributed along NW- to NNW-trending faults, with a number of targets occurring on the bend or most curved sections of the faults as well as being adjacent to granite. The generation of these targets provides an additional data set, which will assist the planning of exploration programs in the region.

5. Discussion

Structural controls on mineralization (hydrothermal deposits in particular) are widespread as reported for many ore deposits around the world (e.g. Taylor, 1984; De Roo, 1988; Baudemont and Fedorowich, 1996; Broadbent et al., 1998; Yigit et al., 2003; Jolley et al., 2004; Haest et al., 2007), and shown by the examples of vein-type mineralization in this paper. At camp and deposit scales, such structural controls are represented by strain localization (shear strain and dilation), the formation of linear structures (faults, shear zones and fractures) and the reactivation of pre-existing structures, which in turn influence fluid flow and mineral precipitation.

The formation and reactivation of linear structures can lead to channelized and localized fluid flow (e.g. Oliver, 1996). This occurs because the deformation and damage (e.g. fracturing) associated with either structural initiation or reactivation can lead to the generation of structural porosity, improved inter-connection of pores or micro-fractures and better linkage of fault networks. These structural improvements imply the development of more efficient fluid conduits for channelized fluid flow, and the significant enhancement of permeability in host rocks for fluid accumulation and transport.

Deformation and structural reactivation can also lead to greater fluid flow velocity and greater flow velocity gradients. First, rock permeability increase of one to two orders of magnitude due to deformation (Zhang and Cox, 2000) can lead to an equivalent increase in fluid flow velocity according to Darcy's law (equation (5)) in reactivated faults and deformed rocks. Second, as demonstrated by previous work (e.g. Schaubs et al., 2006; Zhang et al., 2008) and by the current models, the localization of shear strain during rock deformation and structural reactivation can

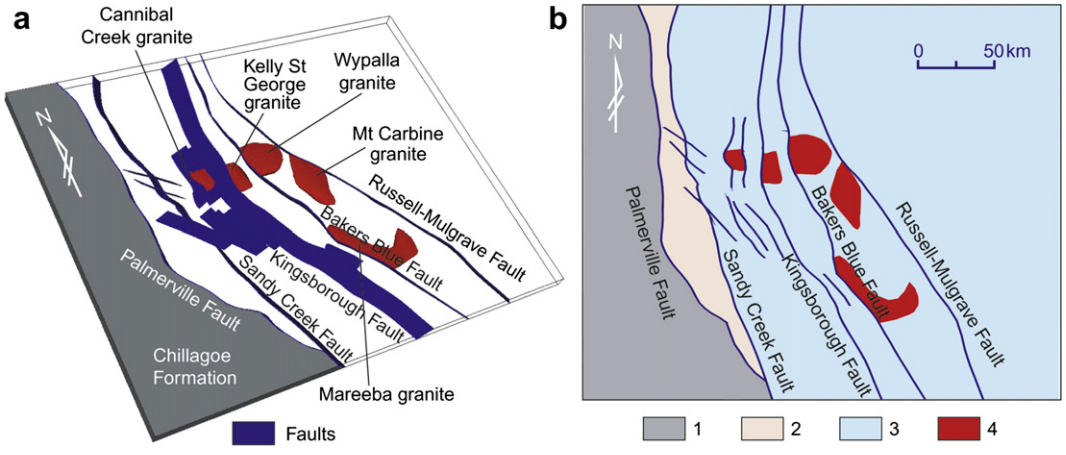

Figure 9 Architecture of the 3D coupled deformation and fluid flow model for the Hodgkinson Province. (a) 3D view of the model geometries with key structural elements highlighted. (b) Plan-view of the model geometries for a horizon about 1 km below the model top surface. Rock units in the model include basement (1), Chillagoe Formation (2), average host rocks (3) and granite (4).

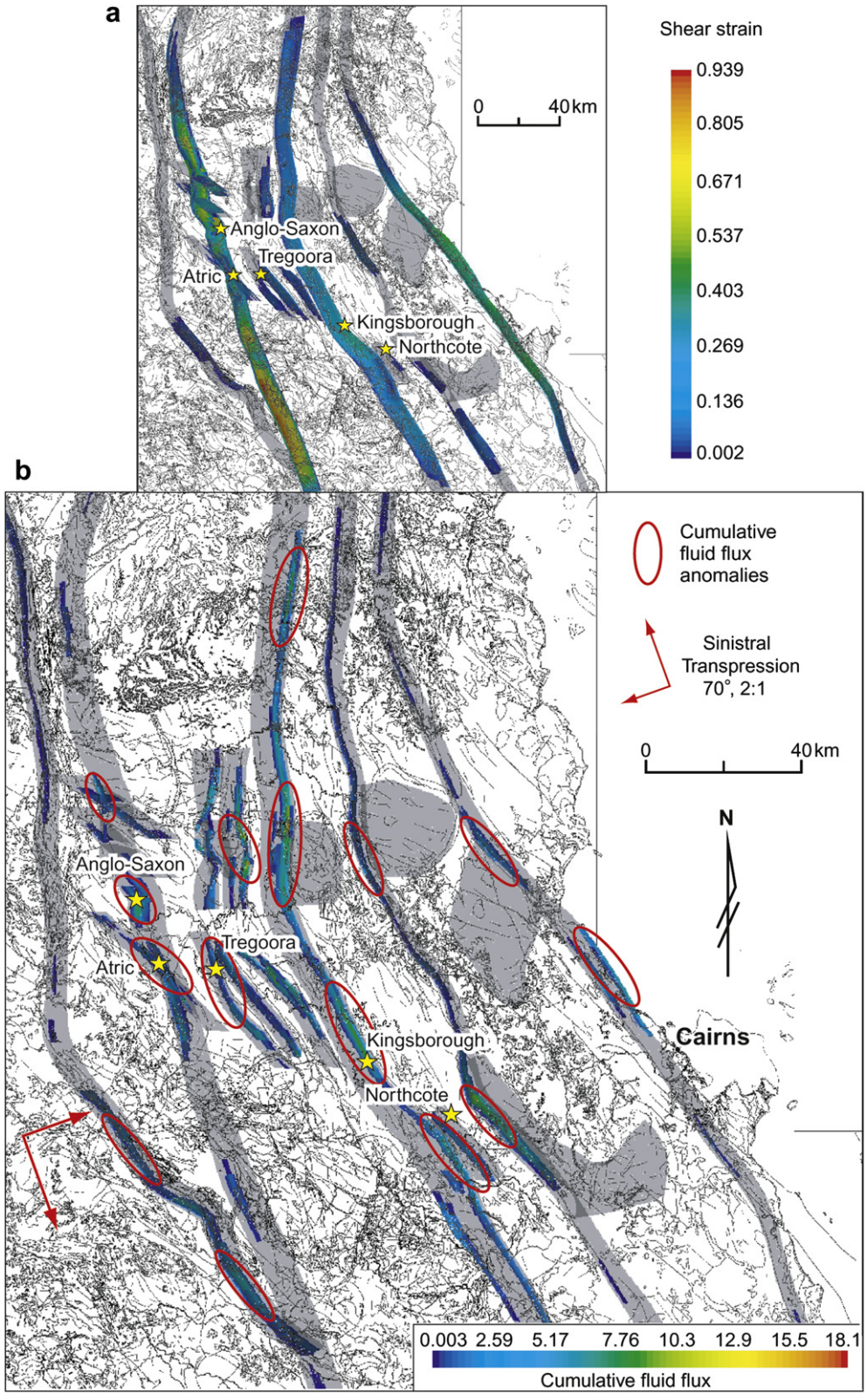

Figure 10 Results of the regional predictive model of the Hodgkinson Province. (a) Shear strain distributions plotted on regional geological outline map. (b) Cumulative fluid flux ($m^3/m^2 \cdot$unit time) distributions plotted on regional map. Stars give the locations of the Anglo-Saxon, Tregoora, Kingsborough and Northcote gold deposits. Grey areas show the locations of the faults and granites simulated in the model. Fluid flux anomalies are highlighted by red circles; those which do not coincide with a known gold deposit represent targets for future exploration. (For interpretation of the references to colour in this figure legend, the reader is referred to the web version of this article.)

cause major dilation in rocks (such as dilation jogs and pull-apart segments of curved fractures and faults). Such dilation will lead to a drop in fluid pressure (equation (7)), fluid focussing and abrupt variation in the fluid velocity gradient in and around dilatant sites. Greater fluid flow velocities and velocity gradient variations will positively affect the rate of mineralization according to equation (6). In addition, dilatancy in deformed rocks also provides favourable space conditions for ore mineral precipitation.

As demonstrated by the results of this study, coupled deformation and fluid flow numerical modelling is capable of predicting structural controls on fluid flow and mineralization. This numerical modelling approach can be used as a predictive tool assisting mineral exploration at camp and deposit scales (e.g. Schaubs et al., 2006; Liu et al., 2010) and regional scales as illustrated by the Hodgkinson Province modelling of this work. However, it should be noted that the desired applicability of the method can only be achieved for a region or deposit where mineralization is dominantly controlled by structural and hydrological factors. Furthermore, due to the domination of structural controls, the interpretation of key structural and stratigraphical configurations for a region should be based on all the available data, so that the best understanding can be achieved for inputs into the numerical models. For areas with major uncertainties on key structures, the numerical modelling can be used as a scenario tool (i.e., a series of models for all the possible structural scenarios; e.g. Potma et al., 2008; Zhang et al., 2010), rather than a definite prediction tool based on only one single speculative structure scenario. The two-phase modelling (i.e., reverse engineering modelling followed by predictive modelling) is also a useful approach, allowing initial application to an area with known mineral deposits (or other reliable geological/structural observations for validation), and then using the information gained, carrying out the further modelling study of a new or larger area.

As described by equation (6), thermal and chemical conditions are two other key factors, together with deformation and fluid flow factors, affecting ore formation or rate of mineralization. The numerical simulations presented here are not suited to cases of thermally-dominated mineralization where thermal gradient and buoyancy variations are important, or for chemically-dominated regimes where chemical gradient variations and their effects on reaction rates play a key role. This reflects the need for further development of the presently available modelling methods in the computational geosciences community. The existing methods only allow for interactions of deformation and fluid flow (e.g. Schaubs et al., 2006; Zhang et al., 2008; this study), thermal transport and deformation (e.g. Lin et al., 2005), thermal transport and fluid flow (e.g. Garven et al., 2001; Yang et al., 2004), or thermal transport-fluid flow-chemical reaction processes (e.g. Zhao et al., 2006; Zhang et al., 2008) for geological systems. Future effort in advancing numerical modelling methodologies needs to be directed towards fully coupled modelling of all of the deformation, fluid flow, thermal and chemical processes. Progress has been recently made by Poulet et al. (2010) simulating the full interactions of the four processes in their simple generic models for a geological system.

6. Conclusions

Structural controls on the formation of hydrothermal deposits are widely observed in many regions across the world, and numerical modelling provides a powerful tool to study such controls. The results of this study show that discrete deformation modelling can realistically simulate the generation of conjugate shear fractures or the development of fracture damage associated with a curved fracture, which match the patterns of the Cu-mineralized vein structures observed at outcrops near the Shilu Cu-deposit, China. The continuum coupled deformation and fluid flow model containing a pre-existing curved fracture also formed patterns consistent with that predicted by the discrete modelling and also with the Cu-vein pattern mentioned above. In addition, the continuum model also provides additional insights into the interaction between deformation and fluid flow. The model shows that the localization of shear strain, development of dilation at the pull-apart segments of the curved fracture and fluid focussing into the dilatant sites controlled the Cu-mineralization observed near the Shilu deposit. As a case study, continuum coupled deformation and fluid flow modelling was applied to the Hodgkinson Province, North Queensland, Australia, based on the architecture derived from the 3D geological model of Geological Survey of Queensland. A series of reverse engineering modelling tests on the Hodgkinson gold field (a smaller area within the Hodgkinson Province, containing several known gold deposits) were first performed to identify the most-likely syn-mineralization kinematic conditions, i.e., a sinistral-transpression regional stress field. The kinematic conditions were then applied to a regional scale model (whole of the Hodgkinson Province). Analysing the results from the regional scale model led to identification of a number of potential gold mineralization targets in the province.

Acknowledgements

This paper has benefited from reviews by Stephen Barnes, Jianwen Yang and an anonymous reviewer. We also thank Alison Ord for discussion and suggestions on the PFC2D modelling, Geological Survey of Queensland and Republic Gold Limited for supporting the work, and Paul Donchak for discussion of the Hodgkinson modelling. Xinyue Chen and Yuejun Wang are thanked for their assistance in drafting Fig. 2.

References

Baudemont, D., Fedorowich, J., 1996. Structural control of uranium mineralization at the Dominique-Peter deposit, Saskatchewan, Canada. Economic Geology 91, 855–874.

Broadbent, G.C., Myers, R.E., Wright, J.V., 1998. Geology and origin of shale-hosted Zn–Pb–Ag mineralization at the Century deposit, northwest Queensland, Australia. Economic Geology 93, 1264–1294.

Cooke, D.R., Hollings, P., Walshe, J.L., 2005. Giant porphyry deposits: characteristics, distribution, and tectonic controls. Economic Geology 100, 801–818.

Cundall, P.A., 2000. Numerical experiments on rough joints in shear using a bounded particle model. In: Lehner, F.K., Urai, J.L. (Eds.), Aspects of Tectonic Faulting. Springer, Berlin, pp. 1–9.

Cundall, P.A., Board, M., 1988. A microcomputer program for modelling large-strain plasticity problems. Numerical Methods in Geomechanics 6, 2101–2108.

Davis, B.K., Bell, C.C., Lindsay, M., Henderson, R.A., 2002. A single late orogenic episode of gold mineralization in the Hodgkinson Province, North Queensland, Australia. Economic Geology 97, 311–323.

De Roo, J.A., 1988. Structural controls on the emplacement of the vein-type tungsten-tin ore at Mount Carbine, Queensland, Australia. Economic Geology 83, 1170–1180.

Dugdale, L.J., 2004. Adding value to exploration—Reducing time and cost to discovery in Western Victoria. Geoscience Australia Record 2004 (9), 39–44.

Edmond, J.M., Paterson, M.S., 1972. Volume changes during the deformation of rocks at high pressures. International Journal of Rock Mechanics and Mining Sciences 9, 161–182.

Garven, G., Bull, S.W., Large, R.R., 2001. Hydrothermal fluid flow models of stratiform ore genesis in the McArthur Basin, Northern Territory, Australia. Geofluids 1, 289–312.

Goldfarb, R.J., Groves, D.I., Gardoll, S., 2001. Orogenic gold and geologic time: a global synthesis. Ore Geology Reviews 18, 1–75.

Groves, D.I., Goldfarb, R.J., Gebre-Mariam, M., Hagemann, S.G., Robert, R., 1998. Orogenic gold deposits: a proposed classification in the context of their crustal distribution and relationship to other gold deposit types. Ore Geology Reviews 13, 7–27.

Haest, M., Muchez, P., Dewaele, S., Franey, N., Tyler, R., 2007. Structural control on the Dikulushi Cu–Ag deposit, Katanga, Democratic Republic of Congo. Economic Geology 102, 1321–1333.

Hobbs, B.E.H., Zhang, Y., Ord, A., Zhao, C., 2000. Application of coupled deformation, fluid flow, thermal and chemical modelling to predictive mineral exploration. Journal of Geochemical Exploration 69–70, 505–509.

Hollings, P., Cooke, D., Clark, A., 2005. Regional geochemistry of tertiary igneous rocks in central Chile: implications for the geodynamic environment of giant porphyry copper and epithermal gold mineralization. Economic Geology 100, 887–904.

Itasca, 2000. FLAC2D: Fast Lagrangian Analysis of Continua. User Manual, Version 4.0. Itasca Consulting Group, Inc., Minneapolis.

Itasca, 2002. PFC2D, Particle Flow Code in 2 Dimensions. User Manual, Version 3.0. Itasca Consulting Group, Inc., Minneapolis.

Itasca, 2004. FLAC3D: Fast Lagrangian Analysis of Continua in 3 Dimensions. User Manual, Version 3.0. Itasca Consulting Group, Inc., Minneapolis.

Jolley, S.J., Freeman, S.R., Barnicoat, A.C., Phillips, G.M., Knipe, R.J., Pather, A., Fox, N.P.C., Strydom, D., Birch, M.T.G., Henderson, I.H.C., Rowland, T.W., 2004. Structural controls on Witwatersrand gold mineralization. Journal of Structural Geology 26, 1067–1086.

Lin, G., Zhang, Y., Guo, F., Wang, Y.J., Fan, W.M., 2005. Numerical modelling of lithosphere evolution in the North China Block: thermal versus tectonic thinning. Journal of Geodynamics 40, 92–103.

Liu, L.M., Zhao, Y.L., Zhao, C., 2010. Coupled geodynamics in the formation of Cu skarn deposits in the Tongling-Anqing district, China: computational modelling and implications for exploration. Journal of Geochemical Exploration 106, 146–155.

Luo, N.H., 1988. Geochemical characteristics and origin of the Guangdong Shilu Cu–Mo deposit. Journal of Guilin College of Geology 8, 77–87 (in Chinese with English abstract).

Malvern, L.E., 1969. Introduction to the Mechanics of a Continuous Medium. Prentice-Hall Inc., New Jersey, 711 pp.

Mandl, G., 1988. Mechanics of Tectonic Faulting. Elsevier, Amsterdam, 407 pp.

Oliver, N.H.S., 1996. Review and classification of structural controls on fluid flow during regional metamorphism. Journal of Metamorphic Geology 14, 477–492.

Ord, A., 1991. Deformation of rock: a pressure-sensitive, dilatant material. Pure and Applied Geophysics 137, 337–366.

Ord, A., Hobbs, B.E., Zhang, Y., Broadbent, G.C., Brown, M., Willetts, G., Sorjonen-Ward, P., Walshe, J.L., Zhao, C., 2002. Geodynamic modeling of the century deposit, Mt Isa Province, Queensland. Australian Journal of Earth Sciences 49, 1011–1039.

Ord, A., Zhang, Y., Hobbs, B.E., Regenauer-Lieb, K., 2004. Brittle fracturing at the laboratory to outcrop scale. Geoscience Australia Record 09, 171–174.

Phillips, O.M., 1991. Flow and Reactions in Permeable Rocks. Cambridge University Press, Cambridge, 296 pp.

Potma, W., Roberts, P.A., Schaubs, P.M., Sheldon, H.A., Zhang, Y., Hobbs, B.E., Ord, A., 2008. Predictive targeting in Australian orogenic-gold systems at the deposit to district scale using numerical modelling. Australian Journal of Earth Sciences 55, 101–122.

Poulet, T., Karrech, A., Regenaur-Lieb, K., Gross, L., Cleverley, J.S., Georgiev, D., 2010. Thermal-mechanical-hydrological-chemical simulations using escript, Abaqus and WinGibbs. In: Abstract for the GeoMod 2010 Conference, 27–29 September, 2010, Lisbon, Portugal.

Schaubs, P.M., Rawling, T.J., Dugdale, L.J., Wilson, C.J.L., 2006. Factors controlling the location of gold mineralisation around basalt domes in the Stawell corridor: insights from coupled 3D deformation-fluid-flow numerical models. Australian Journal of Earth Sciences 53, 841–862.

Schaubs, P.M., Wilson, C.J.L., 2002. The relative roles of folding and faulting in controlling gold mineralization along the Deborah Anticline, Bendigo, Victoria, Australia. Economic Geology 97, 351–370.

Sorjonen-Ward, P., Zhang, Y., Zhao, C., 2002. Numerical modelling of orogenic processes and gold mineralization in the southeastern part of the Yilgarn craton, western Australia. Australian Journal of Earth Sciences 49, 1011–1039.

Strayer, L.M., Hudleston, P.J., Lorig, L.J., 2001. A numerical model of deformation and fluid-flow in an evolving thrust wedge. Tectonophysics 335, 121–145.

Suiker, A.S.J., Fleck, N.A., 2004. Frictional collapse of granular assemblies. Journal of Applied Mechanics 71, 350–358.

Taylor, S., 1984. Structural and paleotopographic controls of lead-zinc mineralization in the Silvermines orebodies, Republic of Ireland. Economic Geology 79, 529–548.

Vermeer, P.A., De Borst, R., 1984. Non-associated plasticity for soils, concrete and rock. Heron 29, 1–64.

Vos, I.M.A., Bierlein, F.P., 2006. Characteristics of orogenic gold deposits in the Northcote district, Hodgkinson Province, north Queensland: implications for tectonic evolution. Australian Journal of Earth Sciences 53, 469–484.

Walsh, J.J., Childs, C., Meyer, V., Manzocchi, T., Imber, J., Nicol, A., Tuckwell, G., Bailey, W.R., Bonson, C.G., Watterson, J., Nell, P.A., Strand, J., 2001. Geometric controls on the evolution of normal fault systems. In: Holdsworth, R.E., Strachan, R.A., Magloughlin, J.F., Knipe, R.J. (Eds.), The Nature and Tectonic Significance of Fault Zone Weakening. Geological Society, London, Special Publications, vol. 186, pp. 157–170.

Yang, J., Large, R.R., Bull, S.W., 2004. Factors controlling free thermal convection in faults in sedimentary basins: implications for the formation of zinc-lead mineral deposits. Geofluids 4, 237–247.

Yigit, O., Nelson, E.P., Hitzman, M.W., Hofstra, A.H., 2003. Structural controls on Carlin-type gold mineralization in the Gold Bar district, Eureka County, Nevada. Economic Geology 98, 1173–1188.

Zhang, S., Cox, S.F., 2000. Enhancement of fluid permeability during shear deformation of a synthetic mud. Journal of Structural Geology 22, 795–806.

Zhang, Y., Lin, G., Roberts, P., Ord, A., 2007. Numerical modelling of deformation and fluid flow in the Shuikoushan district, Hunan Province, South China. Ore Geology Reviews 31, 261–278.

Zhang, Y., Roberts, P., Murphy, B., 2010. Understanding regional structural controls on mineralization at the century deposit: a numerical modelling approach. Journal of Geochemical Exploration 106, 244–250.

Zhang, Y., Schaubs, P.M., Zhao, C., Ord, A., Hobbs, B.E., Barnicoat, A., 2008. Fault-related dilation, permeability enhancement, fluid flow and mineral precipitation patterns: numerical models. In: Wibberley, C.A., Kurz, W., Imber, J., Holdsworth, R.E., Collettini, C. (Eds.), The Internal Structure of Fault Zons: Implications for Mechanical and Fluid-Flow Properties. Geological Society, London, Special Publications, vol. 299, pp. 239–255.

Zhang, Y., Sorjonen-Ward, P., Ord, A., Southgate, P., 2006. Fluid flow during deformation associated with structural closure of the Isa Superbasin after 1575 Ma in the central and northern Lawn Hill platform, northern Australia. Economic Geology 101, 1293–1312.

Zhao, C., Hobbs, B.E., Hornby, P., Ord, A., Peng, S., 2006. Numerical modelling of fluids mixing, heat transfer and non-equilibrium redox chemical reaction in fluid-saturated porous rocks. International Journal for Numerical Methods in Engineering 66, 1061–1078.

Zhao, C., Hobbs, B.E., Ord, A., 2009. Fundamentals of Computational Geoscience. Springer, Berlin, 323 pp.

Zhao, C., Hobbs, B.E., Ord, A., Robert, P.A., Hornby, P., Peng, S.L., 2007. Phenomenological modelling of crack generation in brittle crustal rocks using the particle simulation method. Journal of Structural Geology 29, 1034–1048.

Zucchetto, R.G., Henderson, R.A., Davis, B.K., Wysoczanski, R., 1999. Age constraints on deformation of the eastern Hodgkinson Province, north Queensland: new perspectives on the evolution of the northern Tasman Orogenic Zone. Australian Journal of Earth Sciences 46, 105–114.